Morphological Characterization of Foams during the Filling of Non-Carbonated Beverages

Morphologische Charakterisierung von Schäumen bei der Abfüllung nicht-karbonisierter Getränke

Christopher McHardy[1], Alexander Rudolph[1], Robert Panckow[2], Jordanka Kostova[1], Mirco Wegener[3], Cornelia Rauh[1]

[1] Fachgebiet Lebensmittelbiotechnologie und -prozesstechnik, Technische Universität Berlin, Berlin
[2] Fachgebiet Verfahrenstechnik, Technische Universität Berlin, Berlin
[3] SOPAT GmbH, Berlin

Foam, Foam Morphology, Bubble Size Distribution, Inline-Analysis, Bottling of Beverages
Schaum, Schaummorphologie, Blasengrößenverteilung, Inline-Analyse, Getränkeabfüllung

Abstract

Undesired foaming during high-speed filling of non-carbonated beverages is often observed in practice. To reduce foam formation, the filling dynamics must be adapted to the foaming capacity of the product which in turn reduces the output and economic efficiency of the filling line. The macroscopic stability of these undesired foams is determined by morphological properties of the foam, e.g. the bubble size distribution. At the same time, the entrainment and dispersion of the gas phase in the product is affected by the filling dynamics and the product's material properties. The present contribution deals with the measurement of the morphology of foams arising during the bottling of fruit juices. For this, industrial bottling processes are reproduced in the lab and the forming foams are characterized in real-time with an inline measurement technique which yields 2D photo optical visuals. Automatic image analysis is applied to analyze the shape and size of foam bubbles and determine size distributions with respect to space and time. The results allow conclusions concerning the effect of the volume flow and product properties on the morphology of the foam and provide a basis for the development of actuators for the active control of foaming.

Introduction

Undesired foaming during high-speed filling of non-carbonated beverages like fruit juices is often observed in practice and may cause serious problems in production facilities. For example, contamination of the filling machine with product and microorganisms necessitates frequent cleaning, particularly under aseptic conditions. Another possible consequence of foaming is product underfilling due to the high gas fraction being present in foams and the limited volume of the containers. To reduce foam formation, the filling dynamics are usually adapted to the foaming capacity of the product which in turn reduces the output and economic efficiency of the filling line. Therefore, the prediction and active control of foam formation under industrially relevant conditions are of high interest for producers of non-carbonated beverages.

The observable spatial extent of foam is a consequence of the net balance of foam generation and foam decay (Pilon et al. 2001). Foam generation depends on the foamability of a liquid and the amount of gas entrained. It was shown that the foamability of slags and glasses can be predicted by correlations of non-dimensional numbers containing material properties of the liquid such as dynamic viscosity, surface tension and density (Jiang and Fruehan 1991, Pilon et al. 2001). For fruit juices similar relationships can be derived (McHardy et al. 2018). Concerning the entrainment of a gas phase into the liquid, it can be expected that the configuration of the filling process and the filling speed are the main determining factors. In the present work, a configuration similar to a plunging jet (free jet filling) is considered for which it was shown that gas entrainment in low-viscosity liquids occurs above a critical Weber number in the order of 10^2 which is usually reached in industrial filling processes. Several correlations for the air entrainment rate show a dependence on the Froude or Reynolds numbers (Kieger and Duncan 2012) confirming the observation of stronger foaming at higher filling speed. On short time scales, which are the relevant ones for the filling process (~5-20 s), the dominant phenomenon for foam decay is drainage of the liquid which in turn enhances coarsening and coalescence of foam bubbles (Cantat et al. 2013). A common way to predict drainage is to consider foams as a porous network of liquid-filled channels (Plateau borders) where the flow through the network is governed by Darcy's law (Saint-Jalmes, 2006). Thereby, the microscopic morphology of the foam affects the permeability of the foam and thus, the macroscopic drainage flow. More precisely, for a given liquid the bubble size and curvature affect the flow profile in the Plateau borders which becomes closer to plug flow for larger bubbles (Saint-Jalmes, 2006). On the other hand, as mentioned above, the dynamic evolution of the bubble size is closely related to the local liquid content.

The goal of the present contribution is to determine the morphology of foams forming during the bottling of fruit juices. For this, industrial bottling processes are reproduced in the lab and the forming foams are characterized with an inline measurement technique which yields 2D photo optical visuals. Automatic image analysis is applied to analyze the shape and size of foam bubbles and determine size distributions with respect to space and time.

Material and Methods

Juices and determination of material properties

The experiments were performed with four different commercial juices, namely Multivitamin (MV), Sour Cherry (SC), Pineapple (PA) and Beetroot (BR) juice, each in five-fold repetition. From each juice the mass density, surface tension and dynamic viscosity were determined in threefold repetition at 20 °C. Density was measured with a density meter (oscillating u-tube, Anton Paar DMA 4100 M). The dynamic viscosity was determined in a rheometer (Anton Paar MCR 102) at shear rates between $\dot{\gamma} = 5\ s^{-1}$ and $\dot{\gamma} = 250\ s^{-1}$. The viscosity of SC and BR was found to be independent of the shear rate while for PA and MV shear-thinning behavior and an Ostwald-de Waele relationship was found. The measurement of surface tension was carried out in a force tensiometer (Krüss K11) by means of the plate method. The material properties of the different juices are summarized in Table 1.

Table 1: Material properties of the different fruit juices.

	Density [kg m^{-3}]	Surface Tension [N m^{-1}]	Flow consistency index [Pas^n]	Flow behavior index [-]
MV	1049.23	0.0405	2.048	0.086
PA	1047.80	0.0424	0.015	0.734
SC	1057.88	0.0631	0.00164	1
BR	1041.84	0.0422	0.00147	1

Filling test stand

Fig. 1 depicts details of the filling test stand. The filling process is driven by gravity and initiated by switching the position of a three-way valve (see Fig. 1) from recirculation into the filling mode. The volume flow rate during the filling process is controlled via a pneumatic control valve. The maximum volume flow rate (measured with water) is $\dot{V}_{max} = 0.157 \, L/s$. The filling tube is a DN10 pipe without internals, with its mouth located $32.6 \, cm$ above the bottle base. The test bottle is made of borosilicate glass with an internal diameter of $85 \, mm$ and contains GL threads to connect the sensor probe.
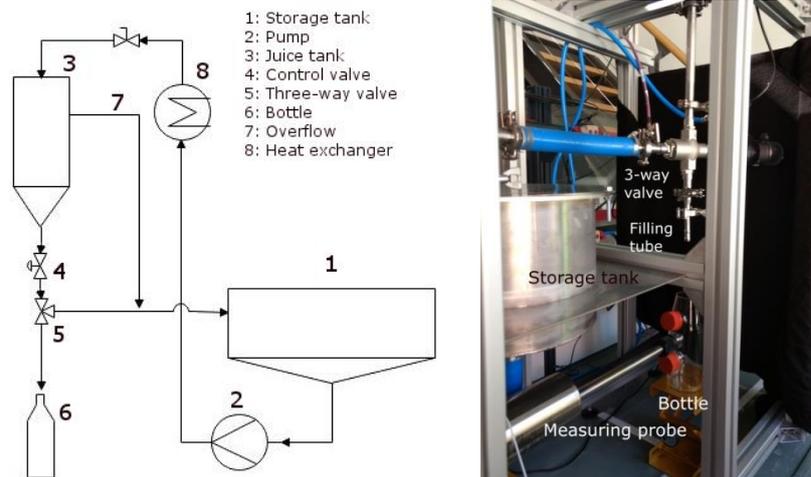

Fig. 1: Filling test stand used in the experiments. Left: schematic drawing of the test stand with all components. Right: photograph of the filling section with the optical measuring probe.

Inline measurement and image processing

Particularly in sensitive and instable systems, the dynamic quantitative size measurement of particles is a major challenge. In contrast to sampling, which is time-consuming and error-prone, an in situ analysis method with high spatial and temporal resolution was selected to detect the particle size distribution of the dispersed phase (Maaß et al. 2012, Panckow et al. 2017). The photo-optical SOPAT measurement technique for particle sizing (*SOPAT GmbH*) used in this study is capable of acquiring raw data (two-dimensional images, see Fig. 2) of the dispersed phase (in this contribution: bubbles) during the running process and measure the sizes and shapes, see Fig. 2 (right).

The measurement system consists of an endoscopic probe connected to a control unit and a workstation. On the latter, automated image analysis is performed to detect and measure the particles projected onto the camera sensor. For the purpose of this study, the probe type "SOPAT *Kr*" was applied to cover the whole spectrum of occurring bubble sizes from two/three-digit microns up to the two-digit millimeter range, see scales in Fig. 2. As can be seen, although some of the investigated juices result in diffuse image material when endoscopically captured, however after prefiltering the software algorithms are capable of detecting the bubbles.

The evaluated photographs of the filling process contained images of the foams and of rising bubbles in the liquid. The exemplary images shown in Fig. 2 are taken from the late stage of the filling process where the foam has already passed the sensor. From these different stages of the filling process the bubble size distribution (BSD) was estimated as well as morphological properties of the foams. The latter contained the number of neighboring bubbles N for each bubble and the arithmetic mean $\langle N \rangle$ for the bubble population in the foam. Moreover, a measure for the sphericity of 2D objects (or projections) is the index of sphericity I_s, which is
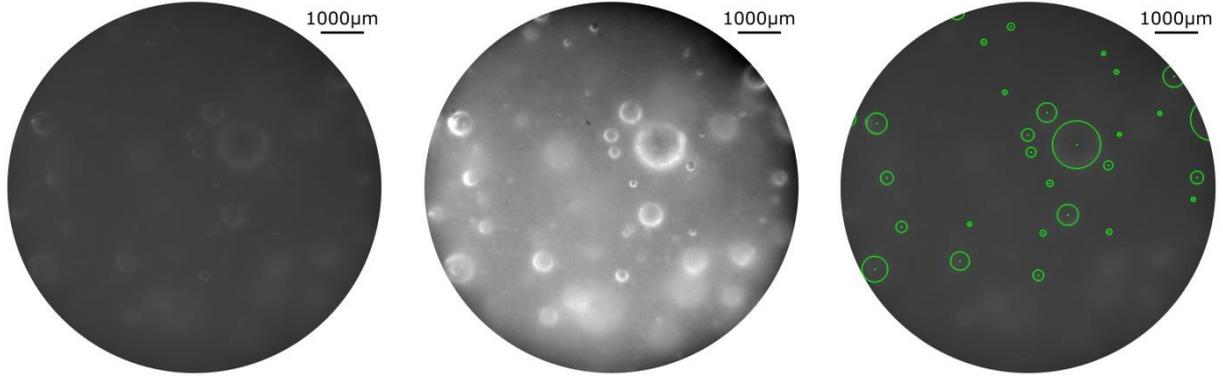
Fig. 2: Raw data acquisition by endoscopic probe "SOPAT *Kr*" (left); contrast-enhanced image (center); detection by SOPAT software (right); pictures recorded in PA juice.

$$I_s = \frac{2}{1 + \pi \dfrac{d_A}{d_p}} \tag{1}$$

where d_A is the area equivalent diameter and d_p the perimeter of the projection area. The polydispersity (Drenckhan and Hutzler 2015) of the bubble population is given by

$$p_{32} = \frac{d_{32}}{(\langle N^3 \rangle)^{1/3}} - 1 \tag{2}$$

where $d_{32} = \sum d_{A,i}^3 / \sum d_{A,i}^2$ is the Sauter mean diameter (SMD). The diagonal Laplacian (LAPD, Pertuz et al. 2013) was computed as an integral property of the recorded images.

Results

Process observation on the macro- and the microscale
Fig. 3 shows the evolution of foam in the bottle during the filling of beetroot juice at different time increments. It can be seen that no foam is observable in the early stage of the filling process whereas the foam thickness increases with the filling time and liquid level. The optical probe at its fixed position in the bottle (see Fig. 1) records during the same time photographs of different characteristic process stages. The liquid jet can be observed in the background until it reaches the window of the sensor. Thereafter, the foam passes the sensor probe and the time it takes is related to the foam height. Thereafter one observes the liquid and suspended gas bubbles within. Therefore the process was divided into the three stages: (1) start of filling, (2) foam, (3) rising bubbles follow-up, see Fig. 3.

Effect of filling speed on the foam height
For a comparison of the spatial extend of foams, the LAPD was computed for each of the 2D photographs. Laplacian based operators are used for edge detection in image processing (Pertuz et al. 2013) and might be useful for analyzing images of foams as their large interface area comes along with an increased number of edges. Fig. 4a shows the computed LAPD signal for PA juice at different filling speeds. Note that the LAPD is plotted over the dimensionless filling time $\tau = t/T$, where T is the total filling time depending on the volume flow. The observation of the foams is accompanied with a prominent peak in the LAPD signal ($0.5 < \tau < 0.8$) and higher filling speed causes a broader peak width. When the entire foam has passed the sensor ($\tau > 0.8$) the LAPD signal shifts towards larger values in case of higher filling speed which might be an indicator for the amount of suspended bubbles in the liquid. Similar observations were made for all juices but different in their extent.

In order to evaluate the foam height from the LAPD signal, a rough estimation can be done based on the width of the major peaks in the signal. More precisely, the foam surface reach-
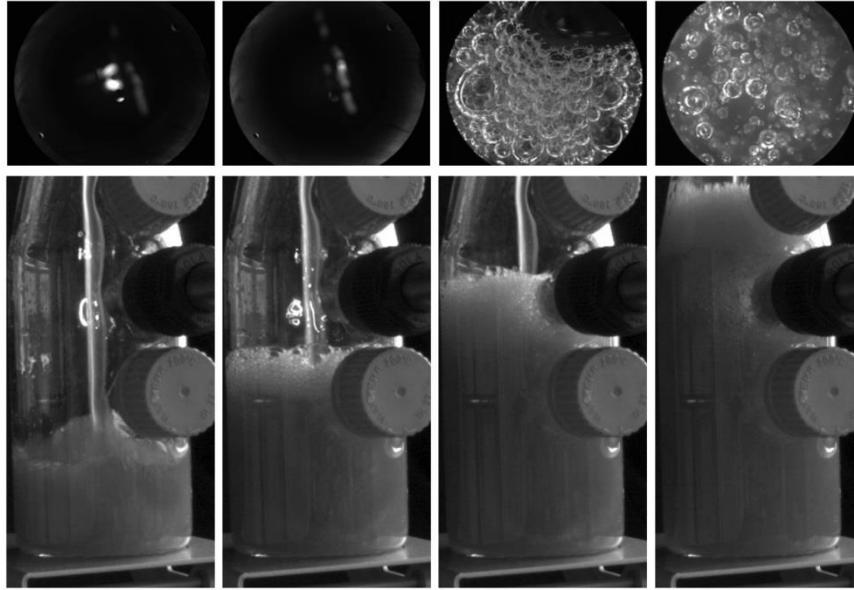
Fig. 3: Different stages during the filling of BR juice at $\dot{V} = 0.14\ L/s$. Images were recorded with the SOPAT Kr probe (top) and a digital camera (bottom) at similar times.

es the lower edge of the sensor window at $\tau = \tau_1$. The foams vertical speed is approximately $u_F = \dot{V}/A_B$, with A_B being the cross-section of the cylindrical part of the bottle. Therefore, the foam surface reaches the window upper edge at $\tau_1 = \tau_0 + H_W/u_F/T$, where $H_W = 0.0103\ m$ is the window height. On the other hand, the juice/foam interface reaches the window upper edge at $\tau_2 = \tau_1 + H_F/u_F/T$ so that the total foam height H_F can be approximated as

$$H_F = Tu_F(\tau_2 - \tau_0) - H_W \tag{3}$$

Fig. 4b depicts the relationship of the estimated foam height to the filling speed. The data show that the foam height increases in good approximation linearly with increasing filling speed. This result deviates from the estimated rates of air entrainment in plunging jet configurations, for which higher order dependencies are reported (Kieger and Duncan 2012). A possible reason for this difference is that a lot of the entrained gas is not present in the foam, rather than being located in bubbles suspended in the liquid. Among the different juices the estimated foam heights differ up to 35 % at highest filling speed. However, it should be emphasized that the estimated foam heights are qualitative measures, although visual inspection during the experiments confirmed the order of a few centimeters foam height (Fig. 3).
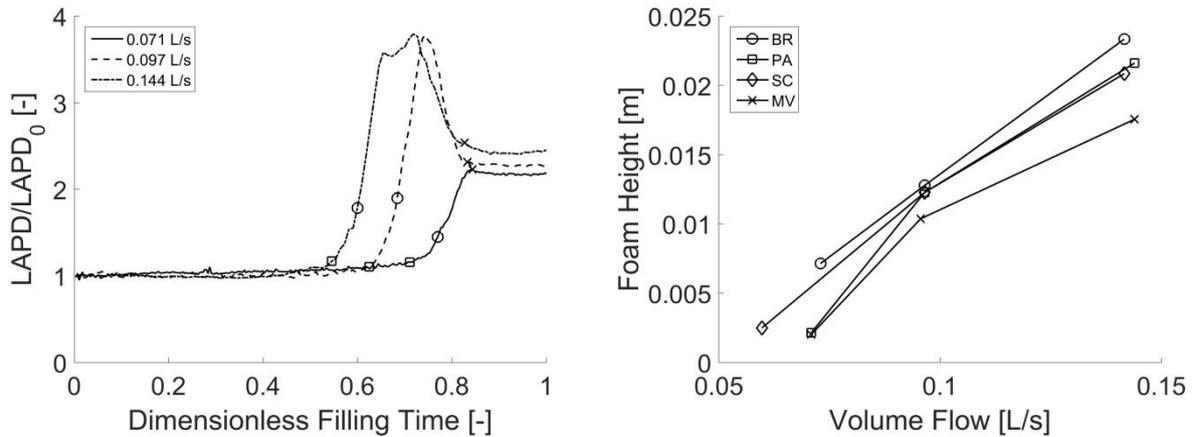

Fig. 4: LAPD raw signal for PA juice at different filling speeds. Symbols denote τ_0 (square), τ_1 (circle), τ_2 (cross) (left); Qualitative estimation of foam heights with respect to the filling speed (right).

Morphology of foams

Important quantities for the characterization of foams are the BSD, the bubble sphericity, polydispersity and the number of neighbors of each bubble (Cantat et al. 2013, Drenckhan and Hutzler 2015). It is important to keep in mind that the observed foams have a 3D structure while all evaluations are restricted to 2D due to the applied observation technique. Consequently, the morphological characterization is based on the area equivalent diameter $d_A =$ ter $d_A = (4A_b/\pi)^{0.5}$, where A_b is the estimated bubble projection area.

Fig. 5a depicts the index of sphericity (see Eq. 1) for bubbles in foams of the different juices. Values close to 1 correspond to a spherical bubble shape and for all juices the bubbles are found to be predominately spherical (see also Fig. 3). Spherical bubbles are characteristic for wet foams with water content $\phi_L \gtrsim 0.15$ (Drenckhan and Hutzler 2015). In such foams coarsening is slow because no bubble intersecting films are present which would enable quick diffusion of gas molecules along the pressure gradient between bubbles of different sizes (Cantat et al. 2013). This underlines that drainage can be expected to be the dominant mechanism that counteracts the foam formation during the filling process.

Fig. 5b shows a comparison of number BSDs in foams of different juices, recorded at $\dot{V} = 0.14\,L/s$. All distributions were computed by means of the Freedman-Diaconis rule from the data of at least 3 images of the respective foams, containing about $300 - 400$ bubbles in total. The majority of bubbles has a diameter between 0.2 and $2\,mm$ in all foams, although it should be mentioned that also some very big bubbles with diameter of up to $10\,mm$ were observed, preferentially located at the free surface of the foams. At $\dot{V} = 0.14\,L/s$ the smallest bubbles exist in PA and SC juice while BR and MV juice contain larger bubbles. With regard to the effect of the filling speed on the BSD, a preliminary result for BR juice shows that at slower filling speed the BDS changes significantly towards smaller bubbles. The extension of this investigation to more filling speeds and juices will be subject of further research.

Fig. 6a depicts the distribution of the number of neighbors of each bubble. It is known that in disordered polydisperse foams bubbles the average number of neighbors is $\langle N \rangle \approx 6$ and in 2D $\langle N \rangle \approx 4$. On the contrary, in 3D for wet ordered foams one finds $6 < \langle N \rangle < 12$ (FCC cell) and for dry disordered foams $\langle N \rangle \approx 13.7$ (Drenckhan and Hutzler 2015). It can be seen that for the foams under investigation most of the bubbles have less than 6 neighbors (in 2D) although some very big bubbles have more than 20 neighbors. This indicates the polydispersity of the foams and moreover that they can be considered as wet and disordered.

Fig. 6b summarizes the topological data of the all foams at volume flow $\dot{V} = 0.14\,L/s$. The average number of neighboring bubbles is very close to the value of $\langle N \rangle \approx 4$ for all foams,
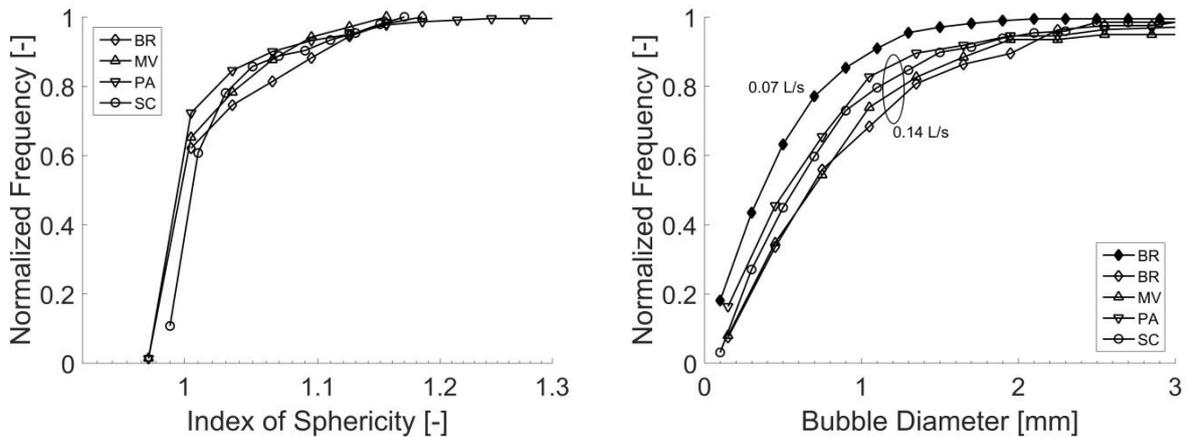

Fig. 5: Distribution of the sphericity for each bubble in foams of different juices at $\dot{V} = 0.14\,L/s$ (left). Number bubble size distributions in foams of different juices (right).
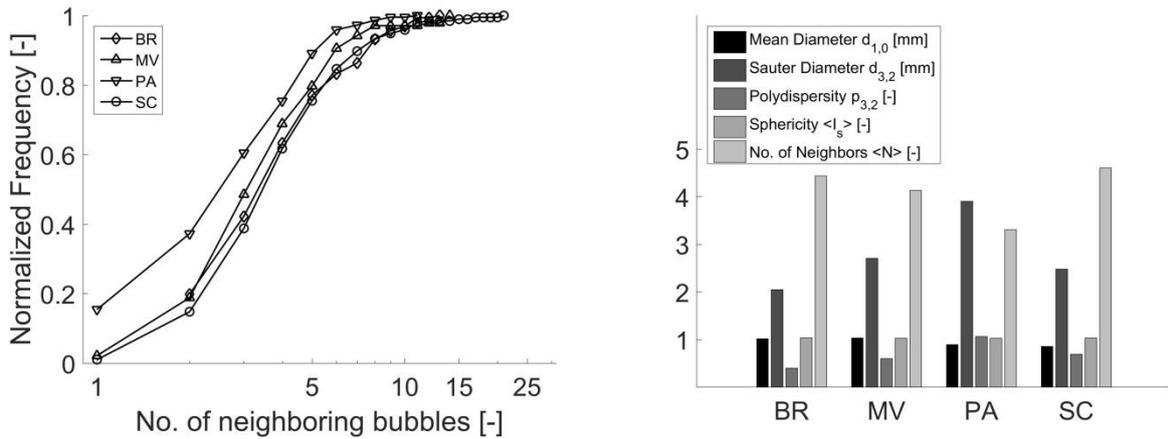
Fig. 6: Distribution of the number of neighboring bubbles for each bubble in different foams at $\dot{V} = 0.14\,L/s$ (left). Averaged morphological properties in foams of juices at $\dot{V} = 0.14\,L/s$ (right).

which is in accordance to the above made statement that the observed foams can be classified as wet. The average bubble size in all foams is $d_{1,0} \approx 1\,mm$. The polydispersity takes values between $0.4 < p_{32} < 1.04$ which must be regarded as high considering that typically $p_{32} < 0.5$ (Drenckhan and Hutzler, 2015). The reason for the ratio $d_{32}/d_{1,0}$ being the highest in PA juice might be that in this juice a lower liquid content was found near the foam surface. Generally, the results indicate that foams forming during the filling process are characterized by disordered spherical bubbles, strong polydispersity and high liquid content.

Bubbly flow

When the foam has passed the sensor probe, one observes rising bubbles in the liquid (see Fig. 3), attaching to the foam when their rising velocity exceeds the foams vertical speed. Fig. 7a depicts the temporal evolution of the bubble Sauter mean diameter (SMD) for different filling speeds, recorded in BR juice. The size of the suspended bubbles depends on the filling speed, although the SMD is much smaller than for foam bubbles. The measurement is in accordance with the observation that in BR foams smaller bubbles were found at reduced filling speed. Fig. 7b compares the temporal evolution of the bubble SMD in different juices at $\dot{V} = 0.14\,L/s$. For bubbles in BR and SC juices larger SMDs were found in comparison to PA or MV juice. It is noticeable that the sequence of the SMDs in the different juices is opposite to the one in the respective foams. This indicates that the ratio of the bubble rise velocity and the rising speed of the liquid could be a determinant for the bubble size in the foams.
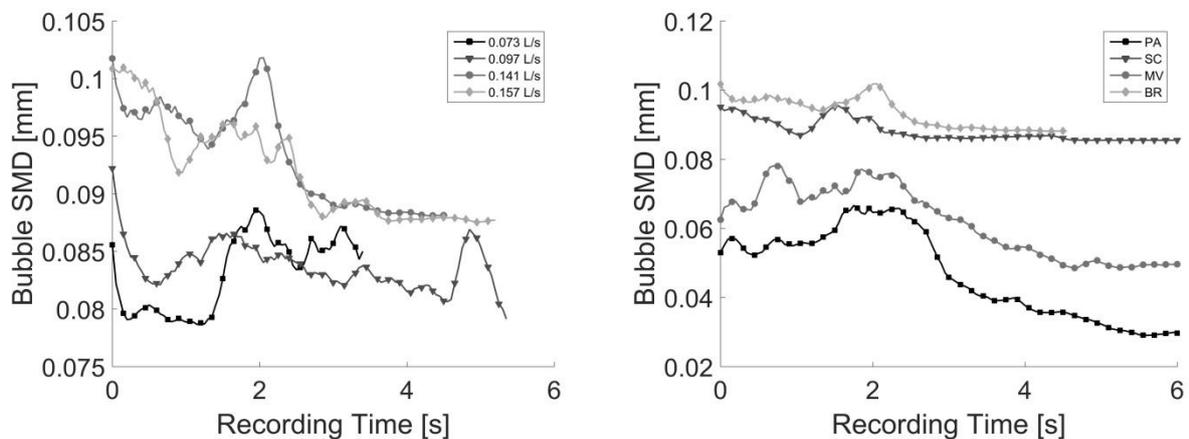

Fig. 7: Effect of filling speed on time course of the bubble SMD in BR juice (left). Time course of the bubble SMD in different juices at $\dot{V} = 0.14\,L/s$ (right). Note the different scaling of the y-axes.

Discussion and Conclusions

In this work foams and bubbles were observed with a photo-optical endoscopic sensor probe during the filling of non-carbonated beverages. It was found that foams are characterized by disordered spherical bubbles, strong polydispersity and high liquid content. The overall foam height depends on the filling speed which is in accordance to the Froude number dependency of gas entrainment in plunging jet configurations. To understand the foam formation in detail, further research must focus on mechanistic explanations for these observations. For example, a strong impact of the filling speed on the BSD in BR juice was observed, coming along with smaller bubbles in the foam at lower filling speed. A possible reason for this can be found in the process of bubble formation which is known to occur at the jet impact point (Kieger and Duncan 2012). On the other hand, entrained bubbles can only contribute to the foam if they reach the liquid surface. In particular, the rise of small bubbles might be affected by jet vortices and at high filling speeds the rise velocity of small bubbles can be small compared to the rise velocity of the liquid. Also the impact of the liquid material properties on the bubble size and foam morphology needs further investigation and thereby possible dependencies on Morton, Weber and Capillary numbers. A direct use of such relations is predicting a foam's height and morphology from the liquid properties and filling process characteristics.

Literature

Cantat, I., Cohen-Abbad, S., Elias, F., Graner, F., Höhler, R., Pitois, O., Rouyer, F., Saint-Jalmes, A., 2013: "Foams – Structure and Dynamics"**.** Oxford University Press

Drenckhan, W., Hutzler, S., 2015: "Structure and Energy of Liquid Foams" Adv Colloid Interface Sci, Vol. 224, pp.1-16

Jiang, A.B., Fruehan, A.B., 1991: "Slag Foaming in Bath Smelting", Metall Trans B, Vol. 22, No. 4, pp. 481-489

Kieger, K.T., Duncan, J.H., 2012: "Air Entrainment Mechanisms in Plunging Jets and Breaking Waves", Annu Rev Fluid Mech., Vol. 44, pp.563-596

Maaß, S., Rojahn, J., Hänsch, R., Kraume, M., 2012: "Automated Drop Detection Using Image Analysis for Online Particle Size Monitoring in Multiphase Systems", Comput. Chem. Eng., 45, pp. 27-37

McHardy, C., Thünnesen, J., Horneber, T., Kostova, J., Hussein, M.A., Delgado, A., Rauh, C., 2018: "Active control of foams by physically based destruction mechanisms" PAMM (submitted)

Saint-Jalmes, A., 2006: "Physical chemistry in foam drainage and coarsening", Soft Matter, Vol. 2, pp. 836-842

Panckow, R.P., Reinecke, L., Cuellar, M.C., Maaß, S., 2017: "Photo-Optical In-Situ Measurement of Drop Size Distributions: Applications in Research and Industry", Oil Gas Sci. Technol., Vol. 72, No. 3, Art.Nr. 14

Pertuz, S., Puig, D., Garcia, M. A., 2013: "Analysis of focus measure operators for shape from focus", Pattern Recognition, Vol. 46, No. 5, pp. 1415-1432

Pilon, L., Fedorov, A.B., Viscanta, A.B., 2001: "Steady-State Thickness of Liquid-Gas Foams", J Colloid Interf Sci, Vol. 242, pp. 425-436